RL-TR-97-249
Final Technical Report
March 1998

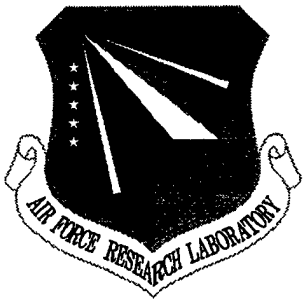

INFRARED IMAGE PROCESSING AND ANALYSIS

Tufts University

Andrzej Brodzik, Paul Kelley, and Elaine Parshall

APPROVED FOR PUBLIC RELEASE; DISTRIBUTION UNLIMITED.

AIR FORCE RESEARCH LABORATORY
ROME RESEARCH SITE
ROME, NEW YORK

This report has been reviewed by the Air Force Research Laboratory, Information Directorate, Public Affairs Office (IFOIPA) and is releasable to the National Technical Information Service (NTIS). At NTIS it will be releasable to the general public, including foreign nations.

RL-TR-97-249 has been reviewed and is approved for publication.

APPROVED: Darin J Leahy

DARIN J. LEAHY
Project Engineer

FOR THE DIRECTOR:

HORST WITTMANN, Director
Electromagnetics & Reliability Directorate

If your address has changed or if you wish to be removed from the Air Force Research Laboratory mailing list, or if the addressee is no longer employed by your organization, please notify AFRL/SNHI, 80 Scott Drive, Hanscom AFB MA 01731-2909. This will assist us in maintaining a current mailing list.

Do not return copies of this report unless contractual obligations or notices on a specific document require that it be returned.

ALTHOUGH THIS REPORT IS BEING PUBLISHED BY AFRL, THE RESEARCH WAS ACCOMPLISHED BY THE FORMER ROME LABORATORY AND, AS SUCH, APPROVAL SIGNATURES/TITLES REFLECT APPROPRIATE AUTHORITY FOR PUBLICATION AT THAT TIME.

REPORT DOCUMENTATION PAGE	Form Approved OMB No. 0704-0188

1. AGENCY USE ONLY *(Leave blank)*	2. REPORT DATE	3. REPORT TYPE AND DATES COVERED
	March 1998	Final Jul 95 - Sep 96

4. TITLE AND SUBTITLE

INFRARED IMAGE PROCESSING AND ANALYSIS

5. FUNDING NUMBERS

C - F30602-95-C-0034
PE - 61102F
PR - 2305
TA - C1
WU - P4

6. AUTHOR(S)

Andrzej Brodzik, Paul Kelley, and Elaine Parshall

7. PERFORMING ORGANIZATION NAME(S) AND ADDRESS(ES)

Tufts University
Electro-optics Technology Center
4 Colby Street
Medford, MA 02155

8. PERFORMING ORGANIZATION REPORT NUMBER

N/A

9. SPONSORING/MONITORING AGENCY NAME(S) AND ADDRESS(ES)

AFRL/SNHI
80 Scott Drive
Hanscom AFB MA 01731-2909

10. SPONSORING/MONITORING AGENCY REPORT NUMBER

RL-TR-97-249

11. SUPPLEMENTARY NOTES

AFRL Project Engineer: Darin J. Leahy/SNHI/(617) 377-5184

12a. DISTRIBUTION AVAILABILITY STATEMENT

Approved for public release, distribution unlimited

12b. DISTRIBUTION CODE

13. ABSTRACT *(Maximum 200 words)*

We present a new algorithm for image restorateion with application to image spectrometry, combining two radically different techniques: the singular value decomposition (SVD) and the method of projections onto convex sets (POCS). The SVD technique is used to obtain an initial estimate of the unknown image and to establish correspondence between the missing data and the spectral description of the image. The iterative method of convex projections is then applied to the estimate, regaining the missing data by enforcing a sequence of constraints on the reconstructed object. We report results of investigations in the recovered image.

We describe an infrared stereo imaging method for the 3-dimensional target tracking of distant moving point sources. In scenes which are typically lacking in significant features, correspondence between the two camera images is simplified by the application of a triple temporal filter to consecutive frames of data. This filter simultaneously accentuates the target and suppresses background clutter. We apply this stereo tracking technique to experimental range measurements in which the target is tracked with sub-pixel precision.

14. SUBJECT TERMS	15. NUMBER OF PAGES
Image restoration, singular value decomposition, projection onto convex sets, infrared stereo imaging, 3 dimensional target tracking	20
	16. PRICE CODE

17. SECURITY CLASSIFICATION OF REPORT	18. SECURITY CLASSIFICATION OF THIS PAGE	19. SECURITY CLASSIFICATION OF ABSTRACT	20. LIMITATION OF ABSTRACT
UNCLASSIFIED	UNCLASSIFIED	UNCLASSIFIED	UL

Standard Form 298 (Rev. 2-89) (EG)
Prescribed by ANSI Std. 239.18
Designed using Perform Pro, WHS/DIOR, Oct 94

Contents

List of Figures

ABSTRACT

We present a new algorithm for image restoration with application to image spectrometry, combining two radically different techniques: the singular value decomposition (SVD) and the method of projections onto convex sets (POCS). The SVD technique is used to obtain an initial estimate of the unknown image and to establish correspondence between the missing data and the spectral description of the image. The iterative method of convex projections is then applied to the estimate, regaining the missing data by enforcing a sequence of constraints on the reconstructed object. We report results of investigations of the SVD-POCS method and demonstrate that the new algorithm leads to significant improvements in the recovered image.

1 INTRODUCTION

The main problem of image reconstruction in infrared image spectrometry is the missing cone in the collected data cube [1,5,6,9,16]. The cone evolves around the zero spatial frequency line, increasing its radius for higher chromatic frequencies. The spectrometer's low spatial frequency 'blindness' results from the finite area of the focal plane array and from the limited dispersion of the prism, which prohibits observation of unbounded objects. The incomplete data phenomenon occurs in many other applications: optical astronomy (where data is lost due to atmospheric turbulence), electron microscopy, SAR and medical CAT (where incomplete view data is acquired). In either case, a unique reconstruction of the observation object is impossible. Use of the Moore-Penrose inverse via SVD offers the minimum norm least square (MNLS) solution; the obtained estimate suffers, however, from poor feature resolution and contains severe artifacts, resulting from the high condition number of the system transfer function matrix.

In an alternative approach, one may avoid the difficulties inherent in inverting a singular matrix and recover the unknown image by utilizing known information about the image. Typically, an initial (often arbitrary) guess about the unknown object is made and then it is subjected to a sequence of corrections, forcing it to satisfy a number of desirable characteristics, such as finite boundary, positivity, etc. This sequence of corrections is applied repetitively, until the reconstruction error becomes sufficiently low. At its simplest, this idea is realized in the form of the Gerchberg-Papoulis procedure [14], where the missing data segment is extrapolated in the Fourier domain, and then used to improve the resolution of the image. The basis for this technique is that a spatially limited object has an analytic Fourier transform, and therefore can be uniquely determined in principle from any finite interval of its spectrum. The Gerchberg-Papoulis approach yields an iterative algorithm, which approaches the solution object by alternating between space domain and Fourier domain. The known parts of the spectrum and the known boundary of the image are imposed on the iterated solution as constraints.

This powerful idea is extended further by the method of projections onto convex sets, where additional *a priori* knowledge about the image (non-negativity, energy, mean, etc.) is incorporated into the algorithm. As a result an increased rate of convergence and an improved performance is achieved, while producing only a modest increase in the computational cost due to implementation of the additional constraints. This advantageous performance/complexity trade-off is of particular importance in image processing situations, where data dimensionality prohibits computationally complex approaches. The main drawback of the POCS method is its sensitivity to the initial guess. It is known that if the initial estimate is not made carefully, the method converges very slowly.

We propose a hybrid algorithm which combines the SVD-based restoration scheme and the POCS method in a way that minimizes the shortcomings of both techniques. The SVD technique is used to

obtain an initial estimate of the unknown image and to establish the correspondence between the condition number of the OTF matrix and the dimension of the transform domain constraint. POCS is then applied to the estimate to reduce blur and artifacts, each POCS iteration producing a corrected version of the previous estimate. The fusion of the two techniques leads to an efficient, robust and general image recovery tool. The combined SVD-POCS approach is viable whenever the optical transfer function model is known prior to image measurement (and therefore SVD computation can be done off-line). It yields significant improvements in the restored imagery, compared to the pseudoinverse method.

2 PROBLEM

An imaging spectrometer reconstructs a three dimensional spatial-chromatic object cube from a sequence of two-dimensional images. The reconstruction can be accomplished in several ways, depending on whether multiplexing of the information is performed in the spatial or chromatic domains, or both. Different multiplexing schemes imply different trade-offs in terms of efficiency, flexibility and complexity of the spectrometer; the numerical formulation of the reconstruction problem however remains in either case essentially the same.

In [13] Mooney proposed a direct vision prism computed-tomography image spectrometry technique. In his approach, the multiplexing is accomplished by rotating the prism. As the prism is rotated, each chromatic slice of the object cube follows a circular path with the radius of the path determined by the prism dispersion. A sequence of spatial, chromatically overlapped images $\{g_m\}$ is thus obtained, each image being a linear superposition of all chromatic slices through the object cube $\{f_n\}$ spatially convolved with a point spread function $\{h_{m,n}\}$

$$g_m(x,y) = \sum_{n=0}^{N-1} h_{m,n}(x,y) ** f_n(x,y), \tag{1}$$

where x and y denote spatial indexes. A Fourier domain equivalent of (1) is

$$\begin{bmatrix} \mathbf{g_0}(\xi,\zeta) \\ \mathbf{g_1}(\xi,\zeta) \\ \cdot \\ \cdot \\ \cdot \\ \mathbf{g_{M-1}}(\xi,\zeta) \end{bmatrix} = \mathbf{H}(\xi,\zeta) \begin{bmatrix} \mathbf{f_0}(\xi,\zeta) \\ \mathbf{f_1}(\xi,\zeta) \\ \cdot \\ \cdot \\ \cdot \\ \mathbf{f_{N-1}}(\xi,\zeta) \end{bmatrix} \tag{2}$$

where the $\mathbf{H}(\xi,\zeta)$ is an $M \times N$ matrix

$$\begin{bmatrix} \mathbf{H_{0,0}}(\xi,\zeta) & \mathbf{H_{0,1}}(\xi,\zeta) & \cdots & \mathbf{H_{0,N-1}}(\xi,\zeta) \\ \mathbf{H_{1,0}}(\xi,\zeta) & \mathbf{H_{1,1}}(\xi,\zeta) & \cdots & \mathbf{H_{1,N-1}}(\xi,\zeta) \\ \cdot & \cdot & \cdots & \cdot \\ \cdot & \cdot & \cdots & \cdot \\ \cdot & \cdot & \cdots & \cdot \\ \mathbf{H_{M-1,0}}(\xi,\zeta) & \mathbf{H_{M-1,1}}(\xi,\zeta) & \cdots & \mathbf{H_{M-1,N-1}}(\xi,\zeta) \end{bmatrix} \tag{3}$$

and $\mathbf{g_m}(\xi,\zeta)$, $\mathbf{H_{m,n}}(\xi,\zeta)$, $\mathbf{f_n}(\xi,\zeta)$ represent two-dimensional discrete Fourier transforms of $g_m(x,y)$, $h_{m,n}(x,y)$ and $f_n(x,y)$, respectively. In shorthand (2) takes the form

$$\mathbf{g} = \mathbf{Hf}. \tag{4}$$

The objective of computed-tomography image spectrometry is to find $\mathbf{f}$, given the measurements $\mathbf{g}$ and the optical transfer function matrix $\mathbf{H}$. Unfortunately, a unique solution to (4) does not in general exist. First, both $\mathbf{g}$ and $\mathbf{H}$ are known only within a finite resolution. Secondly, even an undistorted $\mathbf{g}$ does not completely determine $\mathbf{f}$ in a diffraction-limited system. As a result, the matrix $\mathbf{H}$ becomes singular or ill-conditioned at low spatial frequencies and at high chromatic frequencies, resulting in a region of information ambiguity in the recovered image, known as the 'missing cone' . The situation becomes even worse when the recorded data $\mathbf{g}$ is contaminated by noise, i.e.

$$\mathbf{g} = \mathbf{H}\mathbf{f} + \mathbf{n}. \tag{5}$$

One possible approach which allows exercising some degree of control over instabilities arising from inverting an ill-conditioned matrix, is application of the singular value decomposition (SVD) to $\mathbf{H}$

$$\mathbf{H} = \mathbf{U}\mathbf{w}\mathbf{V}^{\dagger}, \tag{6}$$

where $\mathbf{U}$ is an $M \times N$ column-orthonormal matrix, $\mathbf{w}$ is an $N \times N$ diagonal matrix and $\mathbf{V}$ is an $N \times N$ orthonormal matrix. Since the singularity of $\mathbf{H}$ manifests itself in zero singular values of $\mathbf{w}$, we can easily compute a pseudoinverse of $\mathbf{H}$ as

$$\mathbf{H}^{\dagger} = \mathbf{V}\mathbf{w}^{*}\mathbf{U}^{\dagger}, \tag{7}$$

where an element w^* of the diagonal matrix $\mathbf{w}^*$ is defined as

$$w^* = \begin{cases} 1/w, & w \neq 0, \\ 0, & w = 0. \end{cases} \tag{8}$$

Applying (7) to the noisy situation (5) allows computing an estimate of $\mathbf{f}$

$$\tilde{\mathbf{f}} = \mathbf{V}\mathbf{w}^{*}\mathbf{U}^{\dagger}\mathbf{g} \tag{9}$$

$$= \mathbf{V}\mathbf{w}^{*}(\mathbf{w}\mathbf{V}^{\dagger}\mathbf{f} + \mathbf{U}^{\dagger}\mathbf{n}). \tag{10}$$

The drawback of the pseudoinverse approach is that if one or more entries in the diagonal matrix $\mathbf{w}$ is zero, then there is insufficient information to determine how the measured data should be distributed among chromatic bands and as a result an intra-band crosstalk occurs. Additionally, for small values in $\mathbf{w}$, the noise in (10) is going to be greatly amplified. One way to reduce the noise amplification, is to modify (8)

$$w^* = \begin{cases} 1/w, & w \geq \epsilon_{thr} \\ 0, & w < \epsilon_{thr}, \end{cases} \tag{11}$$

where ϵ_{thr} is a threshold, so that the trade-off between the crosstalk and noise amplification can be balanced. Alternatively, one can apply a form of Wiener filtering to (11), replacing w^* with $w/(w^2 + \epsilon_{thr}^2)$. In either case the balancing between the crosstalk and noise amplification is obstructed by the fact that the threshold can only be roughly estimated, as the image/noise statistics are rarely known with sufficient precision.

Two regularization approaches to the ill-posed (5) are possible: one is based on statistical models of the data (i.e. maximum likelihood, maximum entropy, etc. [10,20]), and another is deterministic, utilizing available *a priori* information about the unknown image. In the next section, we will introduce an iterative algorithm of projections onto convex sets, belonging to the second class of regularization techniques.

3 POCS

The method of projections onto convex sets is a recursive algorithm for finding a point in the intersection of a given sequence of closed convex sets. The method was developed by Bregman [3] and Gubin [8] and adapted to signal processing by Youla [18,19]. POCS was applied by Levi and Stark to image restoration from phase [11], to image restoration from magnitude [12], by Sezan and Stark to limited-angle data restoration [15] and by Trussell to X-ray fluorescence signals [17].

In the simplest case (as will be seen later) POCS reduces to the well-known Gerchberg-Papoulis method. We will provide a summary of the POCS method and list the relevant convex sets without proofs. For details the reader is directed to [19].

The objective of POCS is to find an unknown function f' restricted to lie in the intersection of a given sequence of R closed convex sets

$$C_0 \triangleq \bigcap_{r=1}^{R} C_r. \tag{12}$$

A subset $\mathcal{C}$ of $\mathcal{H}$, where $\mathcal{H}$ is a Hilbert space, is convex, if for any two of its elements x_1 and x_2 it contains the element $x = \mu x_1 + (1-\mu)x_2$, where $0 \leq \mu \leq 1$. A subset $\mathcal{C}$ of $\mathcal{H}$ is closed, if the limit point of any sequence of points in $\mathcal{C}$ is contained in $\mathcal{C}$. Given projection operators P_r associated with closed convex spaces C_r a sequence of functions $\{f_k\}$ is generated by the recursive relation

$$f_{k+1} = P_R P_{R-1} \ldots P_1 f_k = (\prod_{r=1}^{R} P_r) f_k, \tag{13}$$

such that

$$\lim_{k \to \infty} f_k = f', \tag{14}$$

where f' is an element in C_0 that is closest to f. If C_0 contains a single point, the solution is unique. If it contains more than a single point, POCS yields a feasible solution.

The relation (13) can be stated more generally

$$f_{k+1} = (\prod_{r=1}^{R} T_r) f_k, \tag{15}$$

where $T_r = I + \lambda_r (P_r - I)$, $0 < \lambda_r < 2$ and I is the identity operator. The λ_r's are relaxation parameters, and can be used to accelerate the rate of convergence of the algorithm. In general, identification of optimal relaxation parameters, i.e. parameters providing the maximum acceleration, is difficult, and usually suboptimal heuristic choices are made. In a simple situation, however, where only two closed convex sets are used, and one of the projections is linear, a near optimal per-cycle relaxation parameter for the second projection can be calculated [12], that does not require knowledge of the original data f.

The following projection operators are typically used:

1. $\mathcal{C}_1$: The set of all functions in $\mathcal{H}$ that vanish outside a region $B \subset R^2$

$$P_1 f = \chi_B(i,j) f(i,j) = \begin{cases} f(i,j), & (i,j) \in B, \\ 0, & (i,j) \in B^c, \end{cases} \tag{16}$$

where B^c is a complement of B and

$$\chi_B(i,j) = \begin{cases} 1, & (i,j) \in B, \\ 0, & (i,j) \in B^c. \end{cases} \tag{17}$$

2. $\mathcal{C}_2$: The set of all functions in $\mathcal{H}$ whose Fourier transform vanishes outside a frequency region $A \subset R^2$

$$P_2 f \rightarrow \begin{cases} F(u,v), & (u,v) \in A, \\ 0, & (u,v) \in A^c. \end{cases} \tag{18}$$

In the particular case, when only P_1 and P_2 are used, i.e.

$$f_{k+1} = P_2 P_1 f_k, \tag{19}$$

POCS degenerates to the well-known Gerchberg-Papoulis algorithm. Equation (13) can then be rewritten as

$$f_{k+1} = \mathcal{F}^{-1}\{F_0 + (1 - \chi_A)\mathcal{F}\{\chi_B f_k\}\}, \tag{20}$$

where F_0 is the known part of the spectrum of f, and $f_0 = \mathcal{F}^{-1}\{F_0\}$ is the initial estimate of f.

3. $\mathcal{C}_3$: The set of all non-negative functions in $\mathcal{H}$

$$P_3 f = \begin{cases} f, & f \geq 0, \\ 0, & f < 0. \end{cases} \tag{21}$$

4. $\mathcal{C}_4$: The set of all functions in $\mathcal{H}$, whose amplitudes lie in a closed interval $[a,b]$, $0 \leq a < b$

$$P_4 f = \begin{cases} a, & f < a, \\ f, & a \leq f \leq b, \\ b, & f > b. \end{cases} \tag{22}$$

Notice that $\mathcal{C}_3$ is a subset of $\mathcal{C}_4$.

The following projections were additionally considered in this work:

5. $\mathcal{C}_F$: The set of all non-negative area-scaled functions in $\mathcal{H}$

$$P_F f = \begin{cases} \frac{S}{S^+} f, & f \geq 0, \\ 0, & f < 0, \end{cases} \tag{23}$$

where $S = \int\int f(x,y)dxdy$ is the area of f and S^+ is the area of $P_3 f$.

6. C_A: The set of all functions in $\mathcal{H}$, such that

$$P_A f = \alpha f, \quad \alpha = \frac{S^0}{S}, \tag{24}$$

where S^0 is the area of f_{orig}.

7. $C_{T'}$: The set of all functions in $\mathcal{H}$, such that

$$P_{T'} f \leftrightarrow \mathbf{V^\dagger f_{k+1}} = \begin{cases} \mathbf{V^\dagger f_0}, & w \geq \epsilon_{thr}, \\ \mathbf{V^\dagger f_k}, & w < \epsilon_{thr}. \end{cases} \tag{25}$$

This projection operator forms the core of our treatment of the 'missing cone' and is fundamental to the SVD-POCS algorithm: it defines the transform domain extrapolation by expressing the 'missing cone' in terms of singular values of the matrix $\mathbf{H}$. Notice that C_2 is a subset of $C_{T'}$.

8. C_T: The set of all functions in $\mathcal{H}$, such that

$$P_T f \leftrightarrow \mathbf{V^\dagger f_{k+1}} = \frac{w^2}{w^2 + \epsilon_{thr}^2} \mathbf{V^\dagger f_0} + \frac{\epsilon_{thr}^2}{w^2 + \epsilon_{thr}^2} \mathbf{V^\dagger f_k}. \tag{26}$$

This is another version of $P_{T'}$ with smooth thresholding.

We have selected the constraints P_1, P_4, P_A and P_T or $P_{T'}$ to be included in the image recovery algorithm. The finite support constraint P_1 is realized by projecting an $X \times Y$ image through an $X' \times Y'$ ($X' < X$, $Y' < Y$) field stop. At each iteration, pixels residing outside the field stop boundary are reset to a fixed precomputed level. The P_1 constraint can be combined with the P_A constraint, which corrects the zero spatial frequency of the iterated image. The actual value of the dc level of an image is obtained during camera calibration. Additionally, the P_4 constraint can be included in the group of space domain constraints, if estimates of image magnitude limits are available.

In the transform domain we have a choice between P_T and $P_{T'}$. $P_{T'}$ is similar to P_2, except that the spectral correction takes place in the space spanned by columns of the $\mathbf{V}$ matrix. The values of the product $\mathbf{V^\dagger f_0}$ are updated for all triplets (ξ, ζ, n) contained in the 'missing cone' region of the transform space, defined by the condition $w < \epsilon_{thr}$. P_T is a version of $P_{T'}$, which allows for smooth transition between bands (we found that the P_T constraint performs significantly better).

The image reconstruction algorithm consists of two stages (Fig.1.): first, computation of the initial estimate; second, obtaining a refinement of the solution by a series of POCS iterations, in which the recovered image is forced to satisfy predefined characteristics. In the SVD stage, the image estimate $\mathbf{f_0}$ is obtained by taking a product of the adjoint of matrix $\mathbf{H}$ and the collected data vector $\mathbf{g}$, with rows of $\mathbf{U^\dagger g}$ corresponding to small singular values being attenuated by the factor $w^2/(w^2 + \epsilon^2)$. Matrix $\mathbf{V}$ and vector $\mathbf{V^\dagger f_0}$ are stored for later use in the POCS stage. An inverse 2-D DFT is applied to $\mathbf{f_0}$, yielding a starting vector for the iteration.

The POCS iteration includes a sequence of space domain projections followed by a forward 2D DFT, a transform domain projection, and an inverse 2D DFT. The sequence of space domain projections include P_1, P_4 and P_A. The transform domain projection is either $P_{T'}$ or its 'soft' version P_T. This stage requires two operations of matrix-vector multiplications: one for obtaining the product $\mathbf{V^\dagger f_k}$ and one for computing the estimate $\mathbf{f_k} = \mathbf{V}(\mathbf{V^\dagger f_k})$.

The multiplicative complexity of the iterative part of the algorithm is

$$2kXYN(N + 1 + log_2(XY)) \tag{27}$$

where k is the number of iterations, N is the number of colors, and $X \times Y$ is the image size.

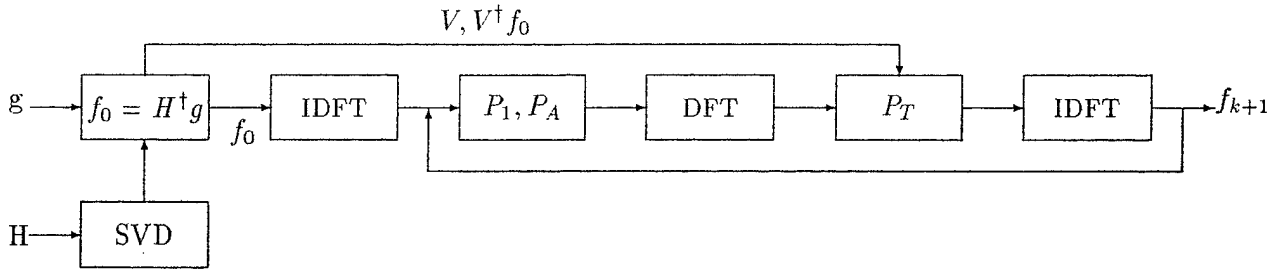

Figure 1: Flowchart of the SVD-POCS algorithm.

4 RESULTS

We have tested two sets of synthesized images: the 'checkerboard' and the 'point source'. The size of both synthetic image arrays was $N \times X \times Y = 8 \times 240 \times 240$, with the field stop being 64×64. The 'checkerboard' image contained a pattern of three sets of pixels of intensities: 10, 300 and 1000. The 'point source' image had a uniform background plane with the set of color intensities $\{650, 600, 550, 500, 450, 400, 350, 300\}$, and a two-pixel target with the set of color intensities $\{650, 600, 550, 500, 450, 400, 1000, 300\}$. In both cases 10 units of white gaussian noise was added to the test image.

We have tested two implementations of the POCS algorithm

$$T1 : f_{k+1} = T_T T_1 f_k, \quad \lambda_{T,1} = 1, 1.9$$

and

$$TAF : f_{k+1} = T_T T_A T_F f_k, \quad \lambda_{T,A,F} = 1, 1.9$$

The basis for comparing results for the synthesized images was the rms error, defined as

$$\epsilon_{rms} = \frac{||f_k - f||}{||f||}.$$

In the case of the 'point source' image, the T1 algorithm ($\lambda_L = 1$) yielded 63% reduction in the rms error after 5 iterations and 84% after 10 iterations (Table 1.). Setting the relaxation parameter $\lambda_{T,1}$ to 1.9 increased the rate of convergence of the algorithm approximately by a factor of two. The accelerated algorithm started to diverge at a moderate rate after about ten iterations.

The TAF algorithm produced spectacularly good results yielding 89% improvement by the second iteration, 93% by the fifth (notice narrowing of the background intensity spread, reduction of blocking effects around the boundary and a large adjustment of the mean in all frames in Fig. 2.), gracefully diverging thereafter. Increasing the relaxation parameter λ_{TAF} to 1.9 actually decreased the rate of convergence, although the results were still better than the results of the T1 algorithm.

In case of the highly textured 'checkerboard' image the improvement yielded by both iterative algorithms was less radical: 45% after 5 iterations and 54% after 10 iterations for T1 algorithm with $\lambda_{T,1} = 1.0$ (Table 2.), resulting in better separation of the three groups of pixels (Fig. 3.). Similarily, as in the case of the 'point source' image, setting $\lambda_{T,1} = 1.9$ provided an approximately twofold increase in the rate

Table 1: Summary of results for image restoration algorithms T1 and TAF (the 'point source').

Iteration number	T1		TAF	
	$\lambda_{T,1} = 1$	$\lambda_{T,1} = 1.9$	$\lambda_{T,A,F} = 1$	$\lambda_{T,A,F} = 1.9$
0	0.1885	0.1885	0.1885	0.1885
1	0.1495	0.1142	0.0392	0.0542
2	0.1225	0.0655	0.0214	0.0227
3	0.1009	0.0407	0.0158	0.0169
4	0.0834	0.0285	0.0143	0.0163
5	0.0693	0.0232	0.0140	0.0163
10	0.0308	0.0193	0.0152	0.0184
15	0.0205	0.0209	0.0168	0.0208
20	0.0194	0.0227	0.0182	0.0228
25	0.0201	0.0244	0.0195	0.0246

of convergence. Somewhat surprisingly the results of TAF and T1 algorithms were nearly identical; the additional constraint did not help nearly as much as for the 'point source' image.

In short, the experiments confirmed that increasing the relaxation parameters in the case of the T1 algorithm improve the rate of convergence significantly. Computation of the optimum-per-cycle parameter as given in [12] yielded marginal improvement in a noisy situation, although earlier experiments have shown excellent results in a noise-free situation. Further research in this area is needed.

Results of the TAF algorithm have shown that certain constraints can yield dramatic improvement for one type of imagery, while having virtually no effect on others (in our case the constraint on zero spatial frequency had a convincing effect on an image with low spatial frequency characteristics). Even though the 'typical' image might be complex in character, design of an adaptive algorithm with a set of adjustable, scenery-dependent constraints might be a reasonable course of action. In absence of information about the image spectrum envelope, it is prudent to use a full set of constraints and properly adjusted relaxation parameters.

5 SUMMARY

In this work, we proposed a hybrid image restoration algorithm which combines the direct inverse approach with an iterative technique that uses *a priori* information about the image. We have tested two iterative methods: the acceleration of the Gerchberg-Papoulis algorithm with variable relaxation parameters and the POCS algorithm in which an additional *a priori* information about low spatial frequencies of the data vector was utilized. Early simulations have shown that application of the hybrid algorithm can lead to significant improvements in data restoration results. It was demonstrated that judicious selection of relaxation parameters can impact the rate of convergence of the two iterative techniques, even in the presence of moderate levels of noise. The theory of convex projections provided a convenient framework by which additional *a priori* information about the data vector could be used to obtain a high quality image in a limited number of iterations.

Table 2: Summary of results for image restoration algorithms T1 and TAF (the 'checkerboard').

Iteration number	T1		TAF	
	$\lambda_{T,1} = 1$	$\lambda_{T,1} = 1.9$	$\lambda_{T,A,F} = 1$	$\lambda_{T,A,F} = 1.9$
0	0.2245	0.2245	0.2245	0.2245
1	0.1796	0.1538	0.1794	0.1539
2	0.1562	0.1295	0.1560	0.1297
3	0.1416	0.1147	0.1415	0.1147
4	0.1315	0.1059	0.1313	0.1055
5	0.1240	0.1000	0.1238	0.0995
10	0.1037	0.0896	0.1036	0.0895
15	0.0961	0.0916	0.0960	0.0921
20	0.0938	0.0966	0.0938	0.0975
25	0.0943	0.1019	0.0943	0.1029

While the SVD-POCS approach shows promise, further work in tuning performance of the algorithm is obviously needed. One parameter, that was observed to have a large effect on the rate of convergence of the iterations, was the singular value threshold. Future research should include design of more sophisticated criteria for threshold selection, including computation of a spatially-weighted optimum-per-cycle threshold. Another possibility is implementation of a multiresolution scheme, in which instead of using an optimum threshold, a weighted sum of images computed at different threshold levels is taken [7]. Finally, computational savings, as well as error reduction, can be potentially achieved by bringing the iterations to a joint time-frequency space, thereby gaining control over the uncertainty principle [4]. These issues are currently under investigation.

6 ACKNOWLEDGMENTS

Effort sponsored by the Air Force Office of Scientific Research and Rome Laboratory, Air Force Materiel Command, USAF, under cooperative agreement #F30602-95-2-0034. The U.S. Goverment is authorized to reproduce and distribute reprints for Govermental purposes notwithstanding any copyright annotation thereon.

7 BIBLIOGRAPHY

[1] H. H. Barrett, *Limited-angle tomography for the nineties*, J. Nucl. Med., 31(10), 1689-1692, 1990,

[2] M. Bertero, *Linear inverse and ill-posed problems*, Advances in Electronics and Electron Physics, Ed. P. W. Hawkes, Vol. 75, Academic Press, 1-120, 1989.

[3] L. M. Bregman, *The method of successive projections for finding a common point of convex sets*, Dokl. Akad. Nauk SSSR, 162(3), 487-490, 1965.

[4] A. K. Brodzik, *The design of discrete Gabor expansion algorithms and an efficient realization of the Gerchberg-Papoulis algorithm in the Zak space*, Ph. D. Dissertation, City University of New York, 1995.

[5] M. R. Descour, *Nonscanning no-moving imaging spectrometer*, SPIE, Vol. 2480, 48-64, 199.

[6] M. R. Descour, *Non-scanning imaging spectrometry*, Ph. D. Dissertation, University of Arizona, 1994.

[7] F. A. Grunbaum, *private communication.*

[8] L. G. Gubin, B. T. Polyak, and E. V. Raik, *The method of projections for finding a common point of convex sets*, USSR Computational Mathematics and Mathematical Physics, 7(6), 1-24, 1967.

[9] D. A. Hayner and W. K. Jenkins, *The missing cone problem in computer tomography*, Advances in computer vision and image processing, Ed. T. S. Huangi, Vol. 1, JAI Press, 83-144, 1984.

[10] R. L. Lagendijk and J. Biemond, *Iterative identification and restoration of images*, Kluwer Academic Publishers, 1991.

[11] A. Levi and H. Stark, *Signal restoration from phase by projections onto convex sets*, J. Opt. Soc. Am., 73, 810-822, 1983.

[12] A. Levi and H. Stark, *Image restoration by the method of generalized projections with application to restoration from magnitude*, J. Opt. Soc. Am., 1, 932-943, 1984,

[13] J. M. Mooney, *Spectral imaging via computed tomography*, Proc. IRIS Passive Sensors, 203-215, 1994.

[14] A. Papoulis, *A new algorithm in spectral analysis and band-limited extrapolation*, IEEE Trans. on Circuits and Systems, CAS-22, 735-742, 1975.

[15] M. I. Sezan and H. Stark, *Image restoration by the method of convex projections: part 2 - applications and numerical results*, IEEE Trans. on Medical Imaging, MI-1, No. 2, 95-101, 1982.

[16] K. C. Tam and V. Perez-Mendez, *Tomographic imaging with limited-angle input*, J. Opt. Soc. Am., Vol. 71, No. 5, 582-592, 1981.

[17] H. J. Trussell and M. R. Civanlar, *The feasible solution in signal restoration*, IEEE Trans. on ASSP, ASSP-32, No. 2, 201-212, 1984.

[18] D. C. Youla, *Mathematical theory of image restoration by the method of convex projections*, Image Restoration: Theory and Application, Ed. H. Stark, Academic Press, 29-77, 1987.

[19] D. C. Youla and H. Webb, *Image restoration by the method of convex projections: part 1 - theory*, IEEE Trans. on Medical Imaging, MI-1, No. 2, 81-94, 1982.

[20] D. Verhoeven, *Limited-data computed tomography algorithms for the physical sciences*, Applied Optics, 32, No. 20, 3736-3754, 1993.

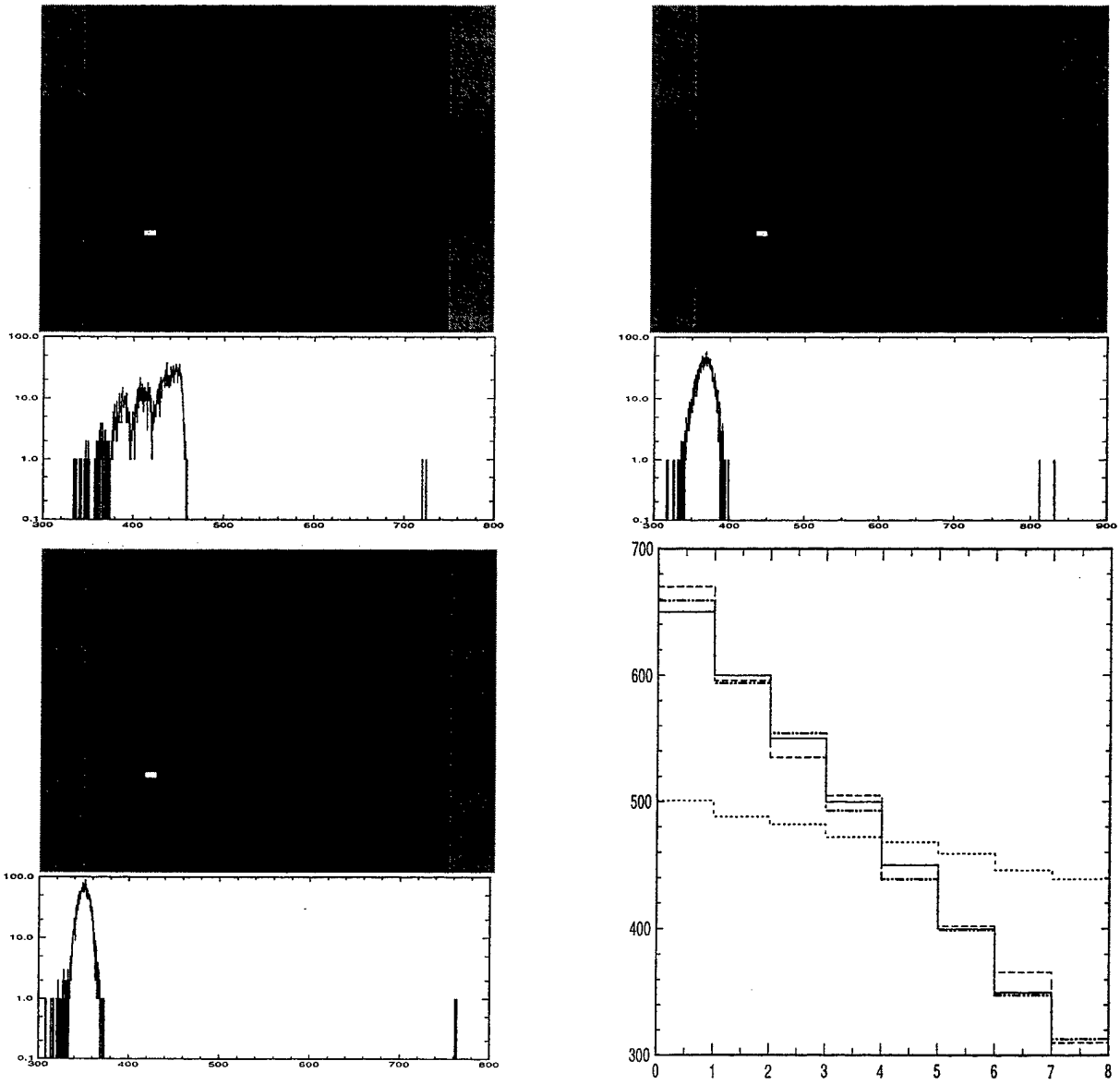

Figure 2: Illustration of the POCS algorithms performance for the 'point source' image (the seventh frame of data and its histogram). (a) result of the SVD algorithm, (b) result of the T1 algorithm for $\lambda = 1.9$ (5th iteration), (c) result of the TAF algorithm for $\lambda = 1$ (5th iteration), (d) comparison of the chromatic series of the central pixel for the SVD algorithm (dotted line), T1 algorithm (dashed line) and TAF algorithm (dashed-dotted line). Solid line marks intensity levels of the original noise-free image.

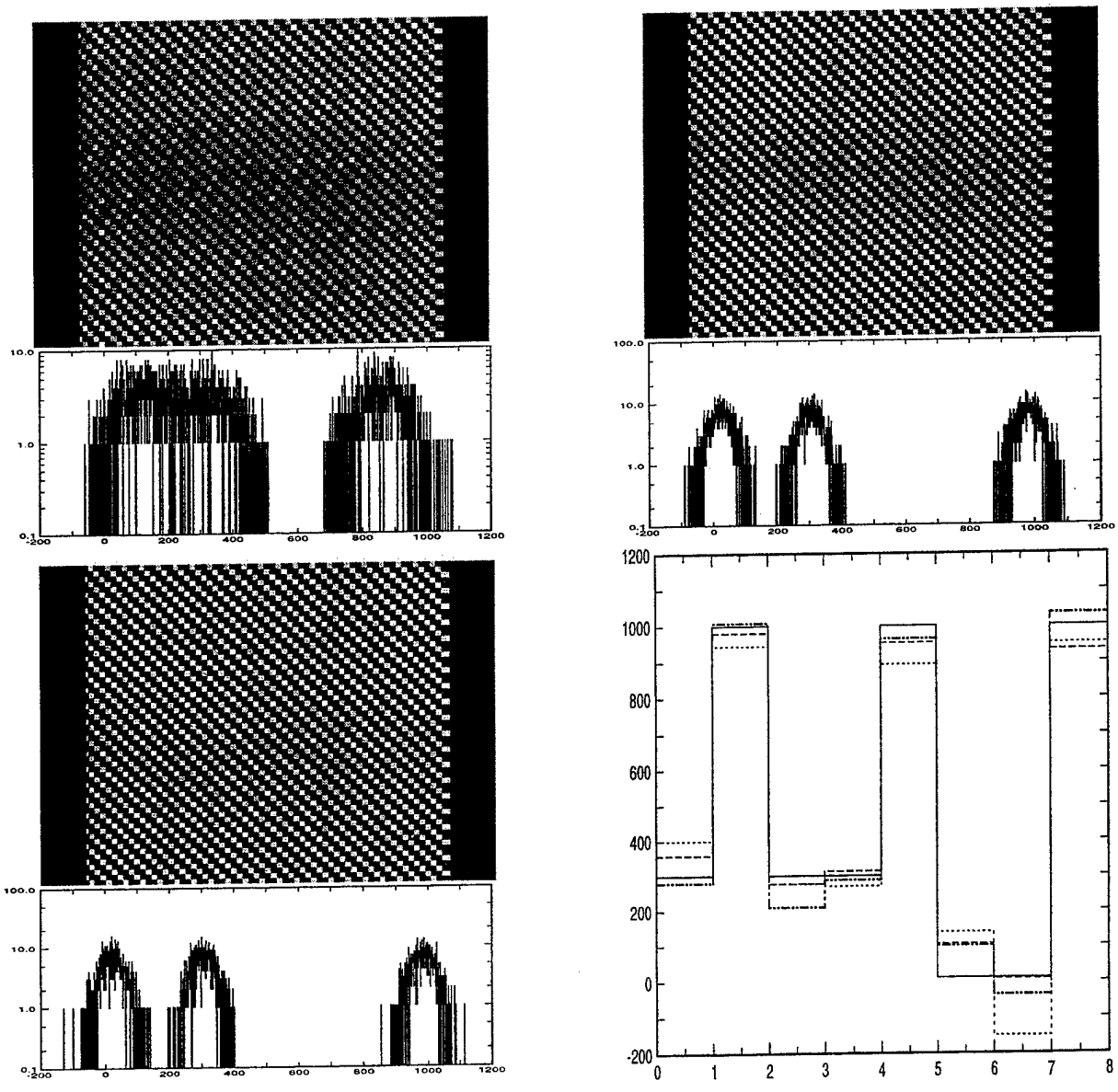

Figure 3: Illustration of the POCS algorithms performance for the 'checkerboard' image (the first frame of data and its histogram). (a) result of the SVD algorithm, (b) result of the T1 algorithm for $\lambda = 1.9$ (10th iteration), (c) result of the TAF algorithm for $\lambda = 1.9$ (10th iteration), (d) comparison of the chromatic series of the central pixel for the SVD algorithm (dotted line), T1 algorithm (dashed line) and TAF algorithm (dashed-dotted line). Solid line marks intensity levels of the original noise-free image.